Earth and Planetary Science Letters 312 (2011) 390–400

Contents lists available at SciVerse ScienceDirect

Earth and Planetary Science Letters

journal homepage: www.elsevier.com/locate/epsl

Molybdenum isotope anomalies in meteorites: Constraints on solar nebula evolution and origin of the Earth

Christoph Burkhardt [a,*], Thorsten Kleine [a,b], Felix Oberli [a], Andreas Pack [c], Bernard Bourdon [a,d], Rainer Wieler [a]

[a] Institute of Geochemistry and Petrology, Clausiusstrasse 25, ETH Zürich, CH-8092 Zürich, Switzerland
[b] Institute for Planetology, University of Muenster, Wilhelm-Klemm Strasse 10, D-48149 Muenster, Germany
[c] Universität Göttingen, Geowissenschaftliches Zentrum, Goldschmidtstrasse 1, D-37077 Göttingen, Germany
[d] Laboratoire de Géologie de Lyon, ENS Lyon, CNRS, 46 Allée d'Italie, F-69364 Lyon, France

ARTICLE INFO

Article history:
Received 12 July 2011
Received in revised form 30 September 2011
Accepted 4 October 2011
Available online 22 November 2011

Editor: R.W. Carlson

Keywords:
Mo isotopes
nucleosynthesis
meteorites
solar nebula
Earth composition

ABSTRACT

The early evolution of the solar nebula involved substantial transport of mass, resulting in mixing and homogenization of isotopically diverse materials that were contributed to the solar system from multiple stellar nucleosynthetic sources. The efficiency of this mixing, as well as its timescale can be quantified by determining nucleosynthetic isotope variations among meteorites and terrestrial planets. Here we present Mo isotopic data for a wide range of samples, including Ca–Al-rich inclusions, chondrites and differentiated meteorites, as well as martian and terrestrial samples. Most meteorites are depleted in s-process Mo relative to the Earth, and only the IAB–IIICD irons, angrites and martian meteorites have terrestrial Mo isotopic compositions. In contrast, most Ca–Al-rich inclusions are enriched in r-process Mo, but one inclusion is characterized by a large s-process deficit. Molybdenum isotopic anomalies in the bulk meteorites correlate with those in Ru exactly as predicted from nucleosynthetic theory, but no obvious correlation is apparent between Mo and Ni anomalies. Therefore, s-process Mo and Ru seem to be hosted in the same carrier, which must be distinct from the carrier responsible for isotopic anomalies in the Fe-group elements (Ni, Cr, Ti). Furthermore, the isotopic heterogeneity in Mo (and other elements) contrasts with the isotopic homogeneity for Hf and Os, indicating that different s-process carriers once existed in the early solar nebula and that only some of these were heterogeneously distributed. The Mo isotopic anomalies of meteorites and their components decrease over time and with increasing size of the parent bodies, providing evidence for a progressive homogenization of the solar nebula. However, the carbonaceous chondrites exhibit larger Mo anomalies than expected for their age, indicating that they received a greater portion of material from the outer solar system (where homogenization was slow) than other meteorite parent bodies and terrestrial planets.
Compared to the meteorites, Earth is enriched in s-process Mo and must have accreted from material distinct from the meteorites. Combined Mo and O isotopic data show that the composition of the Earth cannot be reconstructed by any known combination of meteorites, implying that meteorites may be inappropriate proxies for the isotopic composition of the bulk Earth. This is exemplified by the covariation of ^{92}Mo and ^{142}Nd anomalies in chondrites, showing that the ^{142}Nd deficit of chondrites compared to the accessible Earth may not unequivocally be interpreted as a signature of an early differentiation of the Earth. However, further high precision isotopic data are needed to evaluate the role of chondrites in defining the isotopic composition of the Earth.

1. Introduction

The chemical and isotopic composition of the solar system reflects a particular mixture of matter delivered to the protosolar nebula from multiple nucleosynthetic sources (Burbidge et al., 1957; Wallerstein et al., 1997). Some of the diverse nucleosynthetic components that contributed material to the solar system have been identified via presolar grains in primitive chondrites (e.g., Nittler, 2003). Their highly anomalous isotopic compositions contrast with the generally much more uniform isotope composition of material processed within the Sun's accretion disk. This provides evidence for mixing and homogenization of presolar components in the solar nebula over time. The efficiency and timescales of this mixing are poorly constrained, however, as are the pathways of material transport within the disk. Obtaining such information is key for understanding solar system evolution and for identifying genetic relationships among different planetary bodies,

* Corresponding author. Tel.: +41 44 63 26455; fax: +41 44 63 21827.
E-mail address: burkhardt@erdw.ethz.ch (C. Burkhardt).

0012-821X/$ – see front matter © 2011 Elsevier B.V. All rights reserved.
doi:10.1016/j.epsl.2011.10.010

which may ultimately help constrain the role of meteorites as building blocks of the Earth and other terrestrial planets.

Extent and efficiency of mixing processes in the solar nebula can be investigated by determining isotopic variations that reflect varying proportions of isotopically diverse presolar dust in solar system materials. Isotopic heterogeneity at the bulk meteorite and planetary scale has been observed for a number of elements, including Ti (Trinquier et al., 2007), Cr (Qin et al., 2010; Trinquier et al., 2009), Ni (Regelous et al., 2008), Mo (Dauphas et al., 2002b), Ru (Chen et al., 2010), Ba, Nd and Sm (Andreasen and Sharma, 2007; Carlson et al., 2007). These results contrast with evidence for isotopic homogeneity of Ni (Dauphas et al., 2008), Zr (Schönbächler et al., 2003), Mo (Becker and Walker, 2003b), Ru (Becker and Walker, 2003a), Hf (Sprung et al., 2010) and Os (Yokoyama et al., 2007) that has been reported for some of the same elements. The reasons why planetary-scale nucleosynthetic isotope anomalies seem to exist for some elements but not for others are not known. Many of these anomalies are particularly pronounced in carbonaceous chondrites that contain abundant presolar grains, which led some of the previous studies to emphasize the importance of completely dissolving all presolar phases when investigating the isotope composition of bulk meteorites (Becker and Walker, 2003b; Carlson et al., 2007; Yokoyama et al., 2007).

Molybdenum is a promising element for studying the extent of planetary-scale nucleosynthetic isotopic heterogeneity in the inner solar system. It has seven isotopes of roughly equal abundance that were produced by distinct nucleosynthetic processes, with three Mo isotopes being produced by only one process: ^{92}Mo (p-process); ^{96}Mo (s-process); ^{100}Mo (r-process). This makes Mo isotopes particularly useful for investigating the distribution of different nucleosynthetic components in the solar nebula. Furthermore, Mo occurs in measurable quantities in almost all meteorite groups, permitting a comprehensive assessment of the extent of any isotopic heterogeneity in the inner solar system. However, the extent of Mo isotope anomalies in meteorites is poorly constrained because previous studies obtained disparate results regarding the presence of Mo isotopic anomalies in meteorites (Becker and Walker, 2003b; Dauphas et al., 2002b; Yin et al., 2002).

To assess the origin and extent of Mo isotope variations in the inner solar system, we obtained Mo isotopic data for a wide range of samples, including bulk chondrites, Ca–Al-rich inclusions (CAI), differentiated meteorites as well as martian and terrestrial samples. The new results provide constraints on the timescales and efficiency of mixing processes in the early solar nebula. In addition, the Mo isotope data are important for constraining the provenance of Earth's building blocks, and the role of chondrites as appropriate references for the isotopic composition of the bulk Earth.

2. Analytical techniques

Details regarding sample digestion, chemical separation of Mo, and Mo isotope measurements are given in the Supplementary material. In brief, whole-rock powders of chondrites and achondrites were digested using HF–HNO_3–$HClO_4$ at 180 °C in Savillex beakers on a hotplate. Iron meteorites and chondrite metals were dissolved in 6 M HCl containing traces of HNO_3 at 120 °C. To completely dissolve refractory components and presolar phases, and to assess the effects of different sample digestion methods on the measured Mo isotopic composition, some chondrites and one CAI (A-ZH-10) were fused prior to digestion in acids. Melting of the samples was accomplished by using a CO_2 laser in ultra-pure graphite capsules under oxidizing (atmospheric) or reducing (7% H_2–93% Ar) conditions (Pack et al., 2010).

Molybdenum was separated from the sample matrix using a three-stage ion exchange procedure, resulting in pure Mo cuts with Ru/Mo and Zr/Mo $<3\times10^{-5}$ for most samples. Total procedural blanks were <1 ng Mo and negligible for all samples. Yields as determined by isotope dilution were 70–90%.

Isotope measurements were performed using the Nu Plasma 1700 MC-ICPMS at ETH Zurich at ion beam intensities of $3–4\times10^{-11}$ A on ^{96}Mo, routinely obtained for ~100 ppb Mo. Each measurement consisted of 90 s baseline integrations and 60 Mo isotope ratio measurements of 5 s each. The data were corrected for instrumental mass bias using ^{98}Mo/^{96}Mo = 1.453171 (Lu and Masuda, 1994). Results for other normalization procedures yield internally consistent results (see Supplementary material). Interference corrections for Zr and Ru were usually smaller than 50 ppm, except for the angrite and martian samples, which required corrections of up to 6 ε units. However, tests with doped standard solutions prove the accuracy of our procedures for even larger interference corrections. The Mo isotope ratios are reported in ε^{i}Mo units, which represent relative deviations (parts per 10^4) from the mean of two standard runs bracketing the sample run. The external reproducibility (2SD) of the standard (Alfa Aesar Mo) for normalization to ^{98}Mo/^{96}Mo was ±0.72 ε^{92}Mo, ±0.43 ε^{94}Mo, ±0.26 ε^{95}Mo, ±0.21 ε^{97}Mo and ±0.43 ε^{100}Mo. The accuracy and reproducibility of the Mo isotope measurements were evaluated by repeated analyses of terrestrial standard materials (BCR-2, BHVO-2, SRM82b, SRM129c), all of which yielded Mo isotopic compositions indistinguishable from that of the Mo standard (Table 1).

3. Results

The Mo isotopic data are reported as relative deviation from the Mo isotopic composition of our laboratory standard, which we assume to represent the terrestrial Mo isotopic composition. Although the Mo isotopic composition of Earth's mantle may differ from that of the core due to the addition of a late chondritic veneer to the mantle, the resulting Mo isotopic shifts were probably smaller than our analytical uncertainty. The Mo isotopic composition of the standard (and the terrestrial reference materials analyzed in this study) should, therefore, closely approximate the isotopic composition of terrestrial Mo.

The Mo isotope compositions of samples investigated for this study are given in Table 1 and plotted in Fig. 1 in ε^{i}Mo vs. ^{i}Mo space. Results for normalizations other than ^{98}Mo/^{96}Mo are provided in the Supplementary material. For normalization to ^{98}Mo/^{96}Mo the largest anomalies for all samples are in ε^{92}Mo. The magnitude of the Mo isotope anomalies decreases for most samples in the order ε^{92}Mo > ε^{94}Mo > ε^{95}Mo > ε^{100}Mo > ε^{97}Mo. For some samples, most notably type B CAI, anomalies in ε^{95}Mo are larger than those in ε^{94}Mo, resulting in a distinct Mo isotope pattern with a characteristic kink at ^{94}Mo (Fig. 1). The significance of this kink will be discussed in Section 4.1.

All the investigated type B CAI (A-ZH-1 to -4; A-ZH-10) have indistinguishable Mo isotope anomalies (e.g., ε^{92}Mo ~2.8) and a kink in ^{94}Mo. In contrast, CAI A-ZH-5 exhibits much larger Mo isotope anomalies (ε^{92}Mo ~22) and has a different pattern, i.e., no kink in ^{94}Mo. The petrographic type of this CAI is not yet known, but it is more fine-grained than the type B CAI and exhibits alteration features. While the type B CAI have group I REE patterns, A-ZH-5 shows a group III REE pattern. Furthermore, A-ZH-5 has nucleosynthetic W isotope anomalies, while A-ZH-1 to -4 show no resolvable anomalies in non-radiogenic W isotopes (Burkhardt et al., 2008).

The chondrites investigated for this study have positive Mo isotope anomalies (ε^{92}Mo ~0.5 to ~6.4) with a characteristic w-shaped pattern (Fig. 1). Different samples from the same chondrite group have indistinguishable Mo isotope anomalies. No difference was found in the Mo isotope composition of laser-fused and acid-digested samples (see Table 1), indicating that the Mo isotope anomalies of the chondrites are not caused by incomplete digestion of presolar components. The magnitude of the Mo anomalies in the chondrites decreases in the sequence CM > CR > CV > Tafassasset > CB > CO > CI > OC > EC. No clear correlation is apparent between the Mo isotope anomalies and the physical (e.g., size and abundance of chondrules or CAI; abundance of presolar grains; matrix or porosity) and chemical (e.g., volatile content or redox state) properties of the chondrite groups. For most chondrites

the Mo isotope anomalies are well resolved, but for the enstatite, ordinary and CI chondrites they are at the limit of the analytical resolution achieved in this study. Nevertheless, these chondrites show the same characteristic w-shaped Mo isotope pattern as the other groups, suggesting that all chondrites have Mo isotope compositions different from that of the Earth.

All magmatic iron meteorites, pallasites and IIE irons exhibit positive Mo isotope anomalies ranging from ~2 ε^{92}Mo for the IVB iron meteorites to ~0.7 ε^{92}Mo for the IIE iron meteorites. It is notable that different samples from one iron meteorite group have indistinguishable Mo isotope anomalies, indicating that these isotope anomalies are characteristic for the entire parent bodies of the iron meteorites. The Mo isotope patterns of the iron meteorites are similar to those of the chondrites (i.e., no kink in ^{94}Mo) and only the Eagle Station pallasite shows a slightly different pattern with a possible small kink in ^{94}Mo. The only differentiated meteorites that do not exhibit resolvable Mo isotope anomalies are the non-magmatic IAB–IIICD irons, angrites and martian meteorites.

Finally, no resolvable ^{97}Mo anomalies due to ^{97}Tc decay are present in any of the samples, limiting the solar system initial ^{97}Tc/^{92}Mo to $<1\times10^{-6}$ (Supplementary material).

4. Discussion

4.1. Origin of Mo isotope anomalies in bulk meteorites and CAI

The Mo isotope anomalies in bulk meteorites are most readily accounted for by variable abundances of p-, s- and r-process Mo in these samples. This is illustrated in a ternary plot (Fig. 2), where terrestrial Mo is shown as a mixture of p-, s- and r-process Mo. Also shown in Fig. 2 are the expected Mo isotope anomalies for excesses in p- or r-process isotopes and deficits in s-process isotopes relative to terrestrial Mo. The Mo isotope patterns resulting from these excesses or deficits were calculated using p-, s- and r-process yields for Mo reported in Arlandini et al. (1999), and results are shown for two different normalizations. When ^{98}Mo/^{96}Mo is used for mass bias correction, excesses or deficits in p-, s- or r-process isotopes result in readily distinguishable Mo isotope patterns: (1) a p-process excess is characterized by positive anomalies only in ^{92}Mo and ^{94}Mo; (2) an s-process deficit leads to a distinct w-shaped pattern; and (3) an r-process excess also results in a w-shaped pattern but with an additional kink in ε^{94}Mo. Thus, when using the ^{98}Mo/^{96}Mo normalization it is possible to distinguish between an s-process deficit and an r-process excess. In contrast, for the ^{92}Mo/^{98}Mo normalization the same excesses/deficits produce less characteristic patterns and in most cases also result in smaller Mo isotope anomalies that are more difficult to resolve. For this reason, the Mo isotope data of this study are normalized to the terrestrial ^{98}Mo/^{96}Mo (Table 1).

The comparison of the calculated Mo isotope patterns shown in Fig. 2 to the patterns determined for bulk meteorites and CAI (Fig. 1) reveals that the Mo isotope anomalies of the chondrites and iron meteorites result from a deficit in s-process Mo. Also, CAI A-ZH-5 shows a similar pattern but much larger anomalies. The five type B CAI investigated here have different Mo isotope patterns with a characteristic kink at ε^{94}Mo, which are best accounted for by an excess in r-process Mo isotopes.

To further illustrate the effects of variable proportions of different nucleosynthetic components on the Mo isotope compositions of meteorites, the data are plotted in ε^{i}Mo–ε^{92}Mo space (Fig. 3). Also shown are mixing lines between terrestrial Mo and either a pure s-process or a pure r-process component (Arlandini et al., 1999; Nicolussi et al., 1998). The ε^{94}Mo–ε^{92}Mo and ε^{95}Mo–ε^{92}Mo diagrams illustrate the different effects of an r-process excess and s-process deficit. At a given ε^{92}Mo, addition of an r-process component results in a lower ε^{94}Mo than would subtraction of an s-process component (Fig. 3a). The opposite is observed in ε^{95}Mo–ε^{92}Mo space, where an excess in r-process isotopes results in a higher ε^{95}Mo at a given ε^{92}Mo than a deficit in s-process isotopes. This behavior is responsible for the characteristic kink in the Mo isotope patterns observed for an excess of r-process Mo isotopes, as shown by the type B CAI (Fig. 2).

Also shown in Fig. 3 are linear regressions for the Mo isotope data for bulk meteorites and those obtained for acid leachates of the Orgueil (Dauphas et al., 2002a) and Murchison chondrites (Burkhardt et al., 2011). These regression lines are almost identical to the calculated mixing lines between SiC and terrestrial Mo, indicating that the Mo isotope variations among the bulk meteorites can be attributed to variable proportions of s-process Mo in the different meteorite parent bodies. That the leachate data also plot on the same mixing line than the bulk meteorites indicates that the components responsible for the Mo isotope heterogeneity are present in primitive chondrites.

4.2. Nucleosynthetic Mo isotope anomalies in bulk meteorites — comparison to previous studies

4.2.1. Chondrites

Previous Mo isotope studies did not resolve Mo isotopic anomalies for ordinary and enstatite chondrites (Becker and Walker, 2003b; Dauphas et al., 2002c; Yin et al., 2002), in contrast to the results presented in this study. However, the small Mo isotopic anomalies reported here for ordinary and probably also for enstatite chondrites were not resolvable with the lower precision achievable at the time of these earlier studies. While some of the previous studies reported well-resolved nucleosynthetic Mo isotope anomalies for Allende and Murchison (Dauphas et al., 2002b; Yin et al., 2002), others were unable to reproduce these anomalies and argued that the previously found anomalies do not reflect those of the bulk chondrites but result from an incomplete digestion of isotopically anomalous components (Becker and Walker, 2003b). Most of the carbonaceous chondrites investigated in this study were completely melted using a CO_2 laser prior to digestion in acids. This method should ensure the decomposition of all presolar and refractory components. Although table-top digestion with acids is known to not fully attack presolar grains in chondrites, the Mo isotope composition of acid-digested Murchison measured here is indistinguishable from that obtained for a Murchison sample that has been laser-fused prior to acid digestion (Table 1). This observation suggests that incomplete digestion of presolar grains in chondrites may not have a measurable effect on the Mo isotopic composition. Note, however, that we used higher temperatures and longer digestion times during table-top digestions than previous studies (Dauphas et al., 2002b; Yin et al., 2002). The Mo isotope data for Tafassasset and Gujba provide further evidence that the Mo isotope anomalies in chondrites truly represent those of the bulk rocks. These samples were equilibrated by high temperature events, during which all presolar grains were destroyed. Consequently, all components of these samples should have identical Mo isotopic compositions, so that incomplete digestion could have no effect on the measured Mo isotopic composition. Metals from Gujba and Tafassasset show well-resolved Mo isotope anomalies, demonstrating that bulk carbonaceous chondrites (and related samples) have anomalous Mo isotopic compositions.

The new Mo isotope data for chondrites support earlier conclusions that carbonaceous chondrites have nucleosynthetic Mo isotope anomalies (Dauphas et al., 2002b; Yin et al., 2002) but seem to be inconsistent with the results from Becker and Walker (2003b), who reported no resolvable anomalies for Allende. However, these authors normalized their Mo isotope data to ^{92}Mo/^{98}Mo rather than to ^{98}Mo/^{96}Mo as employed in the present and other previous studies. Fig. 2 shows that the ^{92}Mo/^{98}Mo normalization results in smaller Mo isotope anomalies and less distinctive Mo isotope patterns compared to results obtained with normalization to ^{98}Mo/^{96}Mo. In the ^{92}Mo/^{98}Mo normalization scheme the Mo isotope anomalies of Allende

Table 1
Mo isotopic data for meteorites and terrestrial samples.

Sample		Method[a]	N[b]	Mo[c] (μg/g)	ε^{92}Mo[d]	ε^{94}Mo[d]	ε^{95}Mo[d]	ε^{97}Mo[d]	ε^{100}Mo[d]
Terrestrial standards									
BCR-2	Basalt	Acid	15	249 ± 1	−0.08 ± 0.16	0.00 ± 0.10	0.03 ± 0.06	0.01 ± 0.04	−0.02 ± 0.13
BHVO-2	Basalt	f-ox, f-red	7	2.28 ± 1	−0.04 ± 0.25	−0.22 ± 0.11	−0.03 ± 0.11	−0.09 ± 0.07	−0.01 ± 0.21
SRM 82b	Cast iron	Acid	4	21.50 ± 1	−0.32 ± 0.89	−0.05 ± 0.42	−0.02 ± 0.39	0.00 ± 0.09	−0.39 ± 0.73
SRM 129c	High S-steel	Acid	7	7.46 ± 5	−0.31 ± 0.36	−0.04 ± 0.18	−0.08 ± 0.09	−0.01 ± 0.09	−0.13 ± 0.23
Standard mean					−0.14 ± 0.12	−0.06 ± 0.07	−0.01 ± 0.05	−0.02 ± 0.03	−0.08 ± 0.10
Iron meteorites									
Mundrabilla	IAB	Acid	2	5.17 ± 1	−0.20 ± 0.55	−0.31 ± 0.29	−0.19 ± 0.20	−0.15 ± 0.19	0.10 ± 0.21
Caddo County	IAB	Acid	5	6.53 ± 1	0.08 ± 0.74	0.09 ± 0.43	−0.02 ± 0.27	−0.08 ± 0.17	0.03 ± 0.27
Odessa	IAB	Acid	3	6.33 ± 1	−0.23 ± 1.18	−0.17 ± 0.70	−0.17 ± 0.32	0.01 ± 0.26	0.07 ± 0.21
IAB mean					−0.07 ± 0.34	−0.07 ± 0.23	−0.10 ± 0.12	−0.06 ± 0.09	0.05 ± 0.13
Arispe	IC	Acid	4	6.54 ± 1	0.57 ± 0.31	0.74 ± 0.25	0.17 ± 0.29	0.10 ± 0.12	0.38 ± 0.28
Negrillos	IIAB	Acid	2	6.54 ± 1	1.21 ± 0.34	1.11 ± 0.25	0.38 ± 0.14	0.30 ± 0.12	0.46 ± 0.30
Sikhote Alin	IIAB	Acid	3	6.42 ± 1	1.69 ± 0.81	1.12 ± 0.42	0.56 ± 0.29	0.16 ± 0.16	0.35 ± 0.68
North Chile	IIAB	Acid	2	6.30 ± 1	1.19 ± 0.61	0.99 ± 0.38	0.46 ± 0.23	0.17 ± 0.15	0.61 ± 0.45
IIAB mean					1.41 ± 0.34	1.08 ± 0.17	0.48 ± 0.10	0.21 ± 0.10	0.46 ± 0.19
Carbo	IID	Acid	3	7.76 ± 1	1.29 ± 0.64	0.98 ± 0.36	0.63 ± 0.28	0.46 ± 0.25	0.53 ± 0.54
Miles	IIE	Acid	3	7.37 ± 1	0.64 ± 0.70	0.58 ± 0.05	0.26 ± 0.35	0.23 ± 0.06	0.51 ± 0.38
Watson	IIE	Acid	4	7.01 ± 1	0.76 ± 0.42	0.69 ± 0.46	0.37 ± 0.23	0.14 ± 0.12	0.24 ± 0.36
IIE mean					0.71 ± 0.24	0.64 ± 0.20	0.32 ± 0.13	0.18 ± 0.07	0.35 ± 0.22
Henbury	IIIAB	Acid	3	5.72 ± 1	1.32 ± 0.44	0.90 ± 0.24	0.50 ± 0.26	0.20 ± 0.11	0.20 ± 0.71
Charcas	IIIAB	Acid	2	7.47 ± 1	1.46 ± 0.36	1.06 ± 0.21	0.42 ± 0.16	0.13 ± 0.14	0.41 ± 0.30
Cape York	IIIAB	Acid	3	6.76 ± 1	0.96 ± 0.28	0.84 ± 0.44	0.23 ± 0.60	0.25 ± 0.33	0.33 ± 1.25
IIIAB mean					1.22 ± 0.22	0.92 ± 0.13	0.38 ± 0.17	0.20 ± 0.08	0.30 ± 0.29
Carlton	IIICD	Acid	2	2.64 ± 1	−0.02 ± 0.62	−0.06 ± 0.32	0.04 ± 0.17	−0.06 ± 0.13	0.04 ± 0.31
Stainton	IIIE	Acid	5	7.51 ± 1	1.11 ± 0.58	0.81 ± 0.30	0.39 ± 0.12	0.19 ± 0.11	0.40 ± 0.11
Clark County	IIIF	Acid	3	4.72 ± 1	1.30 ± 1.14	0.98 ± 0.73	0.84 ± 0.80	0.36 ± 0.07	0.70 ± 1.03
Albion	IVA	Acid	3	5.69 ± 1	0.82 ± 0.51	0.59 ± 0.10	0.27 ± 0.15	0.06 ± 0.07	0.21 ± 0.22
Duell Hill	IVA	Acid	3	5.97 ± 1	0.88 ± 0.37	0.68 ± 0.37	0.26 ± 0.26	0.11 ± 0.25	0.12 ± 0.47
Gibeon	IVA	Acid	2	5.02 ± 1	0.66 ± 0.64	0.61 ± 0.40	0.34 ± 0.23	0.20 ± 0.16	0.23 ± 0.44
IVA mean					0.80 ± 0.19	0.63 ± 0.15	0.28 ± 0.09	0.11 ± 0.08	0.18 ± 0.18
Tawallah Valley	IVB	Acid	9	32.14 ± 1	1.99 ± 0.34	1.26 ± 0.18	0.98 ± 0.09	0.51 ± 0.05	0.84 ± 0.20
Santa Clara	IVB	Acid	6	28.43 ± 1	1.91 ± 0.42	1.36 ± 0.16	1.00 ± 0.08	0.49 ± 0.11	0.77 ± 0.22
Tlacotepec	IVB	Acid	3	22.01 ± 1	1.97 ± 1.35	1.42 ± 0.92	0.96 ± 0.32	0.53 ± 0.21	0.91 ± 0.26
Cape of Good Hope	IVB	Acid	4	20.23 ± 1	1.76 ± 0.58	1.32 ± 0.55	1.02 ± 0.09	0.44 ± 0.19	0.71 ± 0.21
IVB mean					1.92 ± 0.18	1.32 ± 0.11	0.99 ± 0.04	0.49 ± 0.04	0.81 ± 0.09
Mbosi	Ungrouped	Acid	5	>1.22 ± 1	1.17 ± 0.67	1.10 ± 0.43	1.02 ± 0.27	0.50 ± 0.20	0.63 ± 0.25
Pallasites									
Brenham	Main group Pal	Acid	6	5.40 ± 1	1.06 ± 0.34	0.85 ± 0.22	0.38 ± 0.14	0.16 ± 0.09	0.20 ± 0.20
Eagle Station	Eagle Station Pal	Acid	6	7.80 ± 1	1.14 ± 0.24	0.85 ± 0.32	0.80 ± 0.14	0.41 ± 0.09	0.79 ± 0.15
Mars and angrites									
Zagami	Shergottite	Acid	1	>0.04 ± 1	0.52 ± 0.75	0.69 ± 0.50	−0.03 ± 0.41	0.02 ± 0.23	−0.14 ± 0.44
DaG476	Shergottite	Acid	1	>0.06 ± 1	−0.12 ± 0.75	0.30 ± 0.50	0.06 ± 0.41	0.18 ± 0.23	0.00 ± 0.44
Mars mean					0.20 ± 0.75	0.49 ± 0.50	0.01 ± 0.41	0.10 ± 0.23	−0.07 ± 0.44
NWA4801	Angrite	Acid	1	>0.13 ± 1	−0.14 ± 0.75	0.09 ± 0.50	−0.12 ± 0.41	0.20 ± 0.23	0.40 ± 0.44
Chondrites									
Orgueil	CI	f-red	2	0.88 ± 1	1.12 ± 0.59	0.79 ± 0.41	0.69 ± 0.23	0.26 ± 0.19	0.44 ± 0.34
Murchison	CM2	Acid	3	1.27 ± 1	6.34 ± 1.31	4.84 ± 0.29	3.13 ± 0.50	1.73 ± 0.51	2.34 ± 0.57
Murchison	CM2	f-red	2	1.02 ± 1	6.66 ± 0.53	5.03 ± 0.37	3.29 ± 0.20	1.65 ± 0.16	2.19 ± 0.32
Murchison	CM2	f-ox	2	0.77 ± 1	6.36 ± 0.55	4.58 ± 0.38	3.09 ± 0.22	1.56 ± 0.17	2.29 ± 0.33
CM mean					6.44 ± 0.39	4.82 ± 0.20	3.17 ± 0.16	1.66 ± 0.14	2.28 ± 0.22
NWA2090	CO3	f-red	2	1.16 ± 1	1.48 ± 0.53	0.92 ± 0.37	0.53 ± 0.20	0.12 ± 0.16	0.35 ± 0.33
Allende	CV3	Acid	4	1.47 ± 1	3.24 ± 0.86	2.35 ± 0.61	1.61 ± 0.07	0.78 ± 0.34	1.19 ± 0.28
Allende	CV3	f-red	4	1.35 ± 1	3.46 ± 0.51	2.53 ± 0.31	1.74 ± 0.20	0.85 ± 0.31	1.01 ± 0.21
CV mean					3.35 ± 0.36	2.44 ± 0.25	1.68 ± 0.09	0.82 ± 0.16	1.10 ± 0.14
NWA801	CR2	f-red	3	1.21 ± 2	3.58 ± 0.64	2.82 ± 0.38	1.73 ± 0.32	0.87 ± 0.36	1.03 ± 0.11
Tafassasset metal	CR anomalous	Acid	2	3.87 ± 1	2.42 ± 0.65	1.54 ± 0.40	1.09 ± 0.24	0.69 ± 0.15	1.18 ± 0.47
Gujba metal	CB	Acid	7	4.47 ± 1	1.74 ± 0.25	1.30 ± 0.26	0.95 ± 0.10	0.47 ± 0.09	0.59 ± 0.23
Bremervörde	H3	Acid	3	1.16 ± 1	0.72 ± 0.53	0.58 ± 0.15	0.34 ± 0.23	0.13 ± 0.30	0.20 ± 0.15
Kernouvé	H6	Acid	2	1.31 ± 1	0.66 ± 0.59	0.57 ± 0.32	0.25 ± 0.22	0.12 ± 0.18	0.37 ± 0.22
Bruderheim metal	L6	Acid	2	1.92 ± 1	0.58 ± 0.65	0.43 ± 0.35	0.12 ± 0.21	0.09 ± 0.15	0.37 ± 0.44
Ladder Creek metal	L6	Acid	3	>5.67 ± 1	0.94 ± 1.94	1.01 ± 1.08	0.29 ± 0.68	0.18 ± 0.05	0.04 ± 0.65
St. Severin metal	LL6	Acid	3	>3.86 ± 1	0.87 ± 1.13	0.74 ± 0.72	0.38 ± 0.50	0.18 ± 0.47	0.08 ± 0.73
OC mean					0.77 ± 0.28	0.69 ± 0.19	0.29 ± 0.10	0.14 ± 0.06	0.19 ± 0.15
Abee	EH4	f-red	3	1.03 ± 1	0.65 ± 1.11	0.61 ± 0.35	0.18 ± 0.35	0.11 ± 0.30	0.31 ± 0.16
Daniel's Kuil	EL6	Acid	4	1.06 ± 1	0.36 ± 0.26	0.30 ± 0.33	0.19 ± 0.20	0.15 ± 0.16	0.01 ± 0.14
EC mean					0.47 ± 0.27	0.42 ± 0.23	0.19 ± 0.12	0.14 ± 0.10	0.12 ± 0.15
CAI									
A-ZH-1	Type B	Acid	5	8.27 ± 1	2.75 ± 0.24	1.30 ± 0.33	1.95 ± 0.10	0.79 ± 0.14	1.08 ± 0.11
A-ZH-2	Type B	Acid	4	7.89 ± 1	2.35 ± 0.62	0.96 ± 0.49	1.96 ± 0.13	1.06 ± 0.17	1.28 ± 0.34

Table 1 (*continued*)

Sample		Method[a]	N[b]	Mo[c] (μg/g)	ε^{92}Mo[d]	ε^{94}Mo[d]	ε^{95}Mo[d]	ε^{97}Mo[d]	ε^{100}Mo[d]
A-ZH-3	Type B	Acid	2	6.59 ± 1	2.17 ± 0.54	0.69 ± 0.37	1.85 ± 0.21	0.93 ± 0.16	0.88 ± 0.32
A-ZH-4	Type B	Acid	5	6.75 ± 1	3.10 ± 0.41	1.45 ± 0.20	2.19 ± 0.13	1.06 ± 0.13	1.23 ± 0.34
A-ZH-10	Type B	f-ox	5	2.15 ± 1	3.15 ± 0.50	1.63 ± 0.24	2.07 ± 0.23	0.93 ± 0.12	1.10 ± 0.28
Type B mean					2.80 ± 0.21	1.29 ± 0.17	2.03 ± 0.07	0.95 ± 0.06	1.14 ± 0.10
A-ZH-5	Fluffy Type A?	Acid	1	5.78 ± 1	21.87 ± 0.72	16.76 ± 0.43	11.06 ± 0.26	6.06 ± 0.21	7.84 ± 0.43

[a] Digestion method: Acid = table-top digestion in acid; f-ox, f-red = laser fusion of sample powder under oxidizing or reducing conditions prior to digestion in acids.
[b] Number of analyses of the same solution.
[c] Uncertainties of Mo concentrations refer to the last significant digit.
[d] Normalized to $^{98}Mo/^{96}Mo = 1.453171$ using the exponential law.; $\varepsilon = (({}^{i}Mo/{}^{96}Mo)_{sample}/({}^{i}Mo/{}^{96}Mo)_{standard} - 1) \times 10^4$. Uncertainties for samples measured more than twice and group means were calculated using $\sigma_{t0.95,n-1}/\sqrt{n}$. For samples measured once, errors are estimated by the standard deviation (2σ) from repeated analysis of the terrestrial standard or the internal propagated error ($\sigma^2_m = \sigma^2_{internal,\ sample} + (\sigma^2_{internal,\ standard\ before} + \sigma^2_{internal,\ standard\ after})/2$), whichever is larger. For samples measured twice the error is estimated by $\sigma_{tot} = (\sigma^2_{m1} + \sigma^2_{excess\ variance\ 1} + \sigma^2_{m2} + \sigma^2_{excess\ variance\ 2})^{0.5}/2$, were $\sigma^2_{excess\ variance}$ = excess variance component of standard measurements at measurement day.

may have simply been too small to be unambiguously resolvable with the precision achievable with the NTIMS technique of Becker and Walker (2003b). For instance, using the $^{92}Mo/^{98}Mo$ normalization, the Mo isotope data for Allende obtained in this study correspond to an ε^{100}Mo value of 2.2 ± 0.2, which overlaps with $\varepsilon^{100}Mo = 0.9 \pm 1.4$ reported by Becker and Walker (2003b). However, for their Allende data Becker and Walker (2003b) also provide results for normalization to $^{98}Mo/^{96}Mo$ and their ε^{92}Mo value of 0.75 ± 0.35 is distinctly lower than the value of 3.35 ± 0.36 obtained here. The reason for this discrepancy is unclear but may be related to sample heterogeneities. For instance, the Mo isotopic composition of Murchison calculated from data for acid leachates and an acid-resistant residue yields slightly smaller Mo isotope anomalies ($\varepsilon^{92}Mo = 4.39 \pm 0.53$; Burkhardt et al., 2011) than that reported here for a different piece of Murchison, most likely reflecting sample heterogeneities at the sampling scale.

The Mo isotope results presented here for Allende and Murchison also differ in some important aspects from those reported by Yin et al. (2002). For both meteorites these authors report ε^{100}Mo values distinctly higher (Allende) and lower (Murchison) than the values determined in the present study. The reasons for these discrepancies are unclear, but it is noteworthy that the Mo isotope patterns of Allende and Murchison reported by Yin et al. (2002) cannot readily be reproduced by subtracting s-process or adding p- and r-process isotopes to terrestrial Mo. On this basis Fujii et al. (2006) proposed that nuclear field shift effects are responsible for the Mo isotope anomalies observed for Murchison by Yin et al. (2002). In contrast, the Mo isotope data for Allende and Murchison reported here are entirely consistent with a deficit in s-process Mo isotopes, indicating that the data from the present study better represent the Mo isotope composition of these meteorites.

4.2.2. Iron meteorites and pallasites

As for the chondrites, previous Mo isotope studies obtained inconsistent results for iron meteorites. While Dauphas et al. (2002b) reported Mo isotope anomalies in iron meteorites, neither Yin et al. (2002) nor Becker and Walker (2003b) could confirm these results and found no resolvable Mo isotope anomalies in iron meteorites. In contrast to the latter two studies, the data presented here reveal widespread Mo isotope anomalies among the iron meteorites,

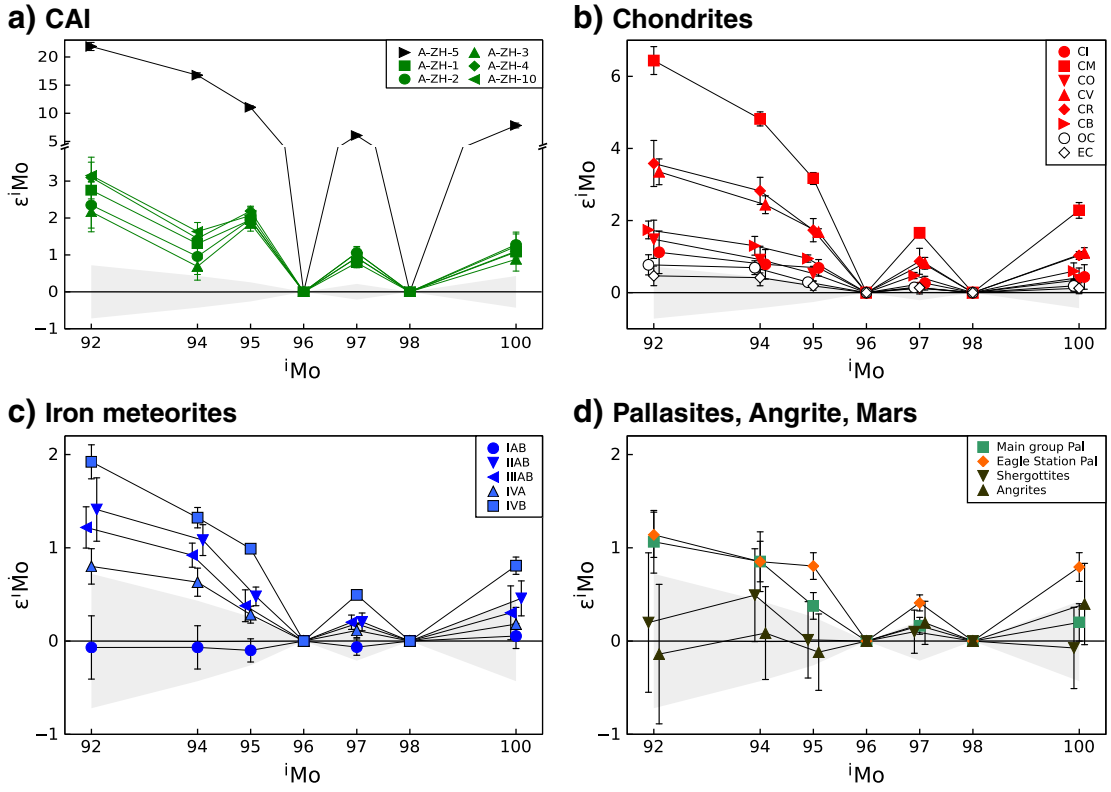

Fig. 1. Mo isotopic data for (a) CAI, (b) chondrites, (c) iron meteorites, and (d) pallasites, angrites and martian meteorites. For clarity, only data of the major iron meteorite groups are shown. Gray area represents the external reproducibility (2SD) of the Mo standard measurements.

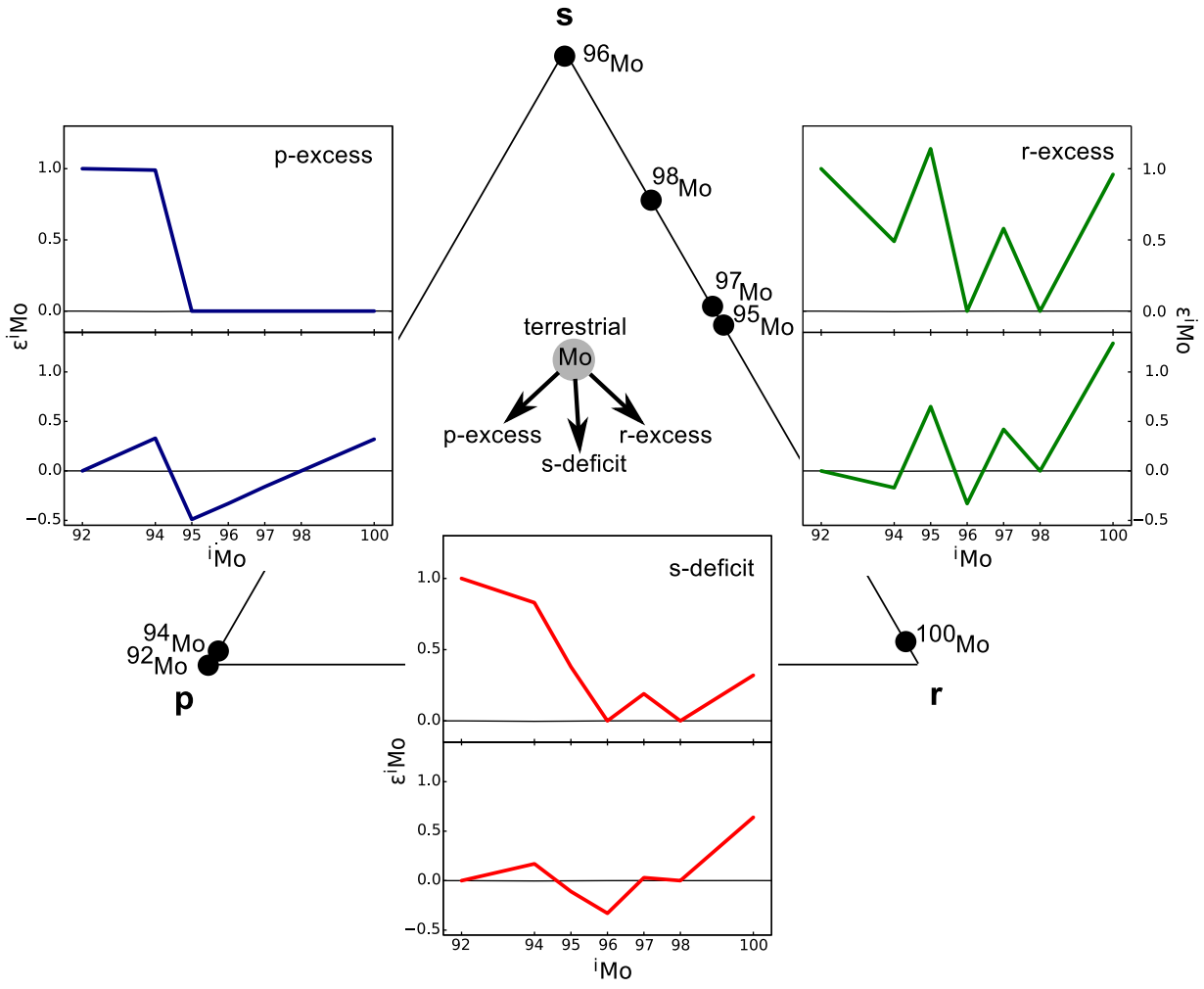

Fig. 2. Ternary plot showing terrestrial Mo as a mixture of three distinct nucleosynthetic components: s-, p-, and r-process Mo. Terrestrial Mo consists of ~50% s-process, ~26% r-process, and ~24% p-process Mo isotopes. A deficit/excess in p-, r-, or s-process Mo relative to terrestrial Mo results in characteristic anomaly patterns that vary depending on the normalization scheme used. Normalization to $^{98}Mo/^{96}Mo$ (upper graphs) results in large anomalies and characteristic patterns: positive $\varepsilon^{92}Mo$ and $\varepsilon^{94}Mo$ for an excess in p-process isotopes; a w-shaped pattern for a deficit in s-process isotopes; and a w-shaped pattern with an additional kink in $\varepsilon^{94}Mo$ for an excess in r-process isotopes. In contrast, the $^{92}Mo/^{98}Mo$ normalization (lower graphs), which was used in some previous Mo isotope studies, results in smaller anomalies and less distinctive patterns. Molybdenum isotope patterns were calculated using s-, p-, and r-process abundances from Arlandini et al. (1999) and scaled to $\varepsilon^{92}Mo = 1$ for the $^{98}Mo/^{96}Mo$ normalization.

which are best accounted for by varying proportions of s-process Mo in the different groups of iron meteorites (see above and Fig. 3). It is noteworthy that even for the IVB irons, which show the largest Mo isotope anomalies among the iron meteorites, the anomalies are at the limit of the analytical resolution that was achievable in the NTIMS studies of Yin et al. (2002) and Becker and Walker (2003b). The discrepancy between the results reported here and those of these earlier studies thus most likely reflects the poorer precision of the NTIMS techniques used in the latter. Furthermore, the use of $^{92}Mo/^{98}Mo$ normalization by Becker and Walker (2003b) made it difficult to resolve the small Mo isotope anomalies present in the iron meteorites.

While the results presented here are in good agreement with (but of higher precision than) those of Dauphas et al. (2002b) for most samples, they are inconsistent for the IIICD irons and the Eagle Station pallasite. For both samples the anomalies reported here are smaller and for the IIICD irons no difference from the terrestrial Mo isotope composition is resolved. Unlike Dauphas et al. (2002b), we found no Mo isotope difference between the IAB and IIICD irons, consistent with the genetic link between these two groups of meteorites (Choi et al., 1995).

4.3. Nucleosynthetic Mo isotope anomalies in CAI

All the investigated CAI exhibit Mo isotope anomalies and all but one (A-ZH-5) show a Mo isotope pattern characteristic for an excess in r-process Mo (w-shaped pattern with kink at ^{94}Mo). In contrast, A-ZH-5 shows a Mo isotope pattern indicative of an s-process deficit (or coupled p- and r-excesses). That only one out of the investigated CAI shows this pattern indicates that CAI with this signature are rare, consistent with the unusual texture and mineralogy of this CAI. The five type B CAI (A-ZH-1 to -4 and A-ZH-10) have indistinguishable Mo isotope anomalies that are also consistent with those of a type B CAI reported by Becker and Walker (2003b), despite the different digestion methods used (acid digestion, Carius tube digestion and laser fusion). This indicates that the measured anomalies represent those of the CAI and are not due to incomplete digestion of isotopically anomalous phases. The evidence for enrichments in r-process Mo isotopes is consistent with similar enrichments for other elements (e.g., Chen et al., 2010; McCulloch and Wasserburg, 1978; Schönbächler et al., 2003) and also with enrichments of neutron-rich isotopes of Ti, Cr and Ni (Birck and Allègre, 1984; Birck and Lugmair, 1988; Niemeyer and Lugmair, 1981).

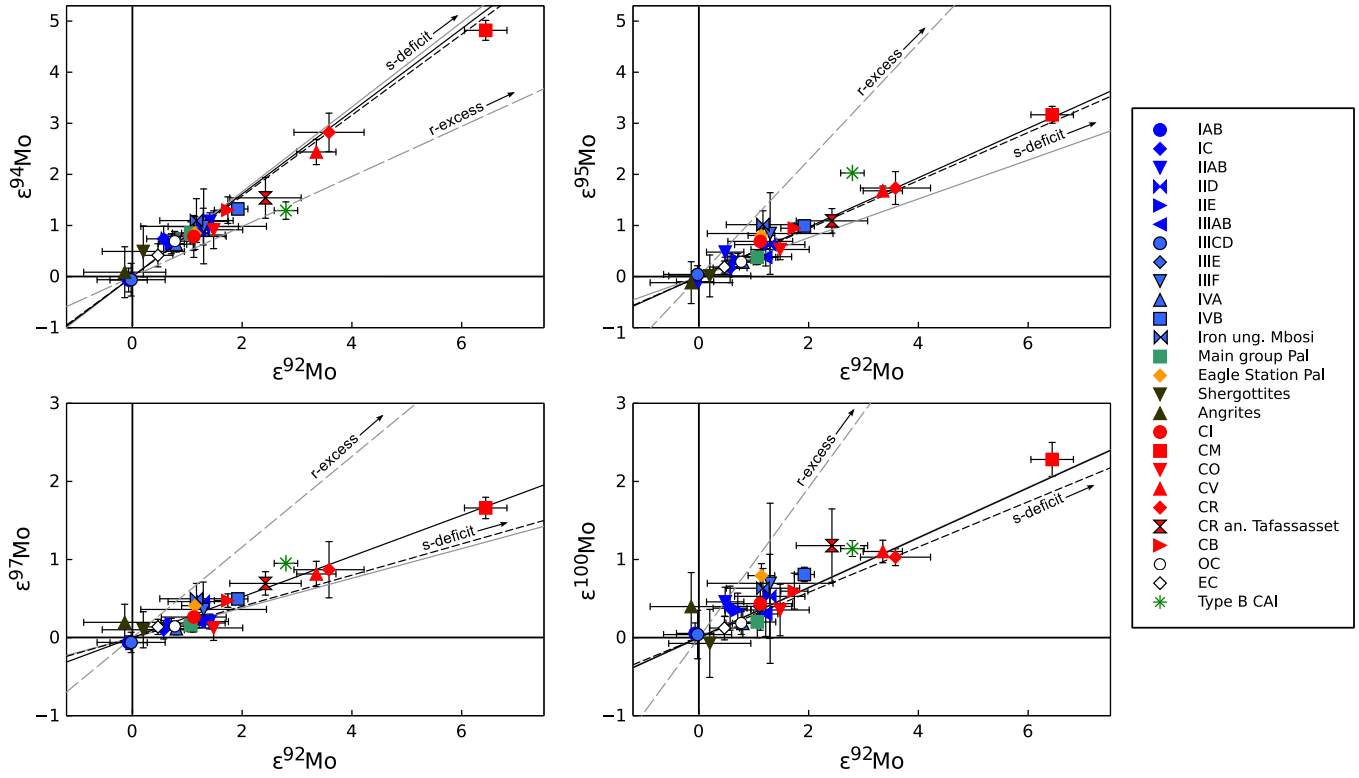

Fig. 3. ε^{92}Mo vs. ε^{i}Mo plots for meteorites and CAI. Symbols are the same as in Fig. 1. Black solid lines are regressions calculated for Mo isotopic data for acid leachates of the Orgueil and Murchison carbonaceous chondrites (Burkhardt et al., 2011; Dauphas et al., 2002a). Gray solid lines represent mixing lines between a theoretical s-process component (Arlandini et al., 1999) and terrestrial Mo, whereas the black dashed lines are mixing lines between s-process Mo as measured in SiC grains (Nicolussi et al., 1998) and terrestrial Mo. Gray dashed lines are mixing lines between terrestrial Mo and an average r-process component (Arlandini et al., 1999). All meteorites plot along mixing lines between terrestrial Mo and an s-process component, whereas type B CAI deviate from these lines towards an excess in r-process isotopes.

However, the observed Mo isotope pattern of type B CAI cannot satisfactorily be fitted by an excess in r-process isotopes alone. This is illustrated in Fig. 3, where type B CAI do not plot on the calculated r-excess line but are shifted towards higher ^{92}Mo abundances. This either suggests that the r-process material added to the CAI precursor derived from a specific r-process source and, hence, had a different composition than the theoretical galactic average r-process component, or that the type B CAI are characterized by excesses in both p- and r-process isotopes.

Two models can account for the observation that CAI formed from material that was isotopically distinct from average solar system matter (e.g., Schönbächler et al., 2003). Either CAI formed from too little material to exactly sample the composition of the average solar system, or they formed from material modified by a late injection of freshly-synthesized material enriched in neutron-rich isotopes. The first of these two options can best account for the isotope composition of CAI A-ZH-5. It is noteworthy that unlike the other CAI, A-ZH-5 displays a similarly shaped Mo isotope pattern as the bulk meteorites albeit with much larger anomalies. As such A-ZH-5 may be interpreted to sample an early heterogeneity of the nebular material the meteorites and planets subsequently formed from.

In contrast, all type B CAI are enriched in neutron-rich isotopes and as such exhibit a Mo isotope pattern distinct from those of the bulk meteorites. Consequently, they do not seem to simply sample an early heterogeneity of the solar nebula. Their composition more likely arose from a late injection of neutron-rich material into the solar nebula.

4.4. Distribution of s-process components in the solar nebula

Our observation of heterogeneous Mo isotope compositions in bulk meteorites is consistent with evidence for planetary-scale nucleosynthetic isotope anomalies for other elements, including Cr and Ti (Trinquier et al., 2009), Ni (Regelous et al., 2008), Ru (Chen et al., 2010), Ba, Sm and Nd (Andreasen and Sharma, 2006; Carlson et al., 2007). Fig. 4a shows that Mo and Ru isotope anomalies correlate exactly as predicted from nucleosynthetic theory for variable deficits in s-process isotopes. A linear regression of ε^{100}Ru vs. ε^{92}Mo yields a slope of -0.46 ± 0.06, in excellent agreement with a slope of -0.44 calculated by Dauphas et al. (2004) from s-process abundances of Mo and Ru. This provides strong evidence that the Mo and Ru isotopic anomalies reflect a heterogeneous distribution of a common s-process carrier.

The heterogeneous distribution of s-process isotopes of Mo and Ru contrasts with a homogeneous distribution of s-process isotopes in other elements, such as for example Hf and Os (Sprung et al., 2010; Yokoyama et al., 2007; Yokoyama et al., 2010). This implies that Mo and Ru are hosted in different carriers than Hf and Os. Furthermore, there is no obvious correlation between Mo and Ni isotopic anomalies in bulk chondrites and iron meteorites (Fig. 4b), although the latter are well correlated with those for Cr and Ti (Regelous et al., 2008; Trinquier et al., 2009). This suggests that different host phases contributed to the isotopic variability in the Fe-group elements on the one hand and Mo (and Ru) on the other. This observation is not surprising because these elements are produced in different stellar environments and thus likely condensed in different host phases.

Dauphas et al. (2002b, 2004) proposed that varying proportions of SiC grains in the meteorites are responsible for the Mo and Ru isotope anomalies. However, this interpretation is difficult to reconcile with the absence of nucleosynthetic Os isotopic variations that would be expected for a heterogeneous distribution of SiC (Yokoyama et al., 2007). To investigate this issue further we modeled the effects of varying proportions of SiC on the isotopic composition of Mo, Ba and Nd, using the isotopic composition of SiC [s-process abundances

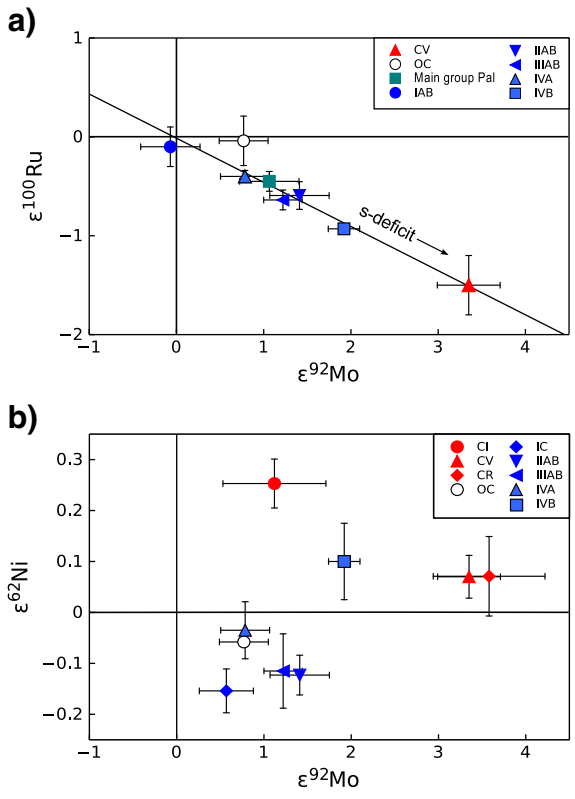

Fig. 4. Plots of (a) ε^{92}Mo vs. ε^{100}Ru and (b) ε^{92}Mo vs. ε^{62}Ni in iron meteorites and chondrites. Ru isotopic data from Chen et al. (2010), Ni isotopic data from Regelous et al. (2008). (a) The regression of the Mo and Ru isotopic data yields a slope of -0.46 ± 0.06, indistinguishable from the slope calculated for variable s-process deficits in these samples (Dauphas et al., 2004). This provides strong evidence that the Mo and Ru anomalies are caused by a heterogeneous distribution of a common s-process carrier. (b) Mo and Ni isotopic anomalies in iron meteorites and chondrites are not correlated, indicating that Mo and Ni reside in different carriers, which were produced in distinct stellar environments.

from the stellar model of Arlandini et al. (1999)] and Mo, Ba and Nd concentrations of 40, 28 and 4.2 ppm [mean values of single grain measurements (Amari et al., 1995; Kashiv et al., 2001)]. A 5 ppm (wt.) SiC deficit can reproduce the observed Mo isotopic anomalies in Allende and would result in Ba and Nd isotopic anomalies (+44 ppm in ^{135}Ba; +21 ppm in ^{137}Ba; −40 ppm in ^{142}Nd; +42 ppm in ^{148}Nd) comparable to those measured for high pressure-digested and fused Allende samples [+38 ppm in ^{135}Ba; +25 ppm in ^{137}Ba (Andreasen and Sharma, 2007); −40 ppm in ^{142}Nd; +21 ppm in ^{148}Nd (Carlson et al., 2007)]. However, while there is reasonable agreement for Allende, the model fails to match the measured isotopic composition of Murchison. A 9 ppm deficit in SiC reproduces the Mo isotopic anomalies in Murchison, but the resulting Ba isotopic anomalies are twice as high (e.g., +79 ppm in ^{135}Ba) as those measured for Murchison [e.g., +40 ppm in ^{135}Ba (Andreasen and Sharma, 2007)]. These calculations suggest that SiC may not be the only carrier responsible for the planetary-scale variability of s-process isotopes. The stepwise dissolution of the Orgueil and Murchison chondrites reveals that s-process Mo is preferentially released by leaching with HCl–HF (Burkhardt et al., 2011; Dauphas et al., 2002a). This provides further evidence that SiC is not the only carrier of s-process Mo, and suggests that yet unidentified presolar silicates may be another important carrier.

In summary, planetary-scale isotopic heterogeneities in the solar nebula appear to be caused by a heterogeneous distribution of at least three distinct carriers. One of these is responsible for heterogeneities in s-process isotopes of Mo, Ru and perhaps also Ba and Nd. This carrier must be poor in Hf and Os, or, alternatively, has isotope compositions for these elements similar to the average composition of the inner solar nebula. The anomalies in the neutron-rich isotopes of Ti, Cr, and Ni must be contributed by different host phases, as must be the deficiencies in p-process isotopes of Sm (and possibly Nd) in carbonaceous chondrites (Andreasen and Sharma, 2006; Carlson et al., 2007). Collectively these data highlight the importance of identifying the distinct presolar components present in the solar nebula for understanding the origin of planetary-scale isotopic heterogeneities.

4.5. Solar nebula heterogeneity in time and space

Dynamical models of solar system evolution predict large-scale mixing and transport of material in the solar nebula, resulting in a homogenization of isotopically diverse components over time (Boss, 2008; Ciesla, 2009). Isotope anomalies in planetary bodies caused by a heterogeneous distribution of presolar components may thus arise either (i) due to an early accretion, i.e., at a time when the solar nebula had not been completely homogenized, or (ii) by a late injection of freshly synthesized and isotopically anomalous material. Alternatively, isotopic anomalies in bulk meteorites may reflect more localized processes, either in the solar nebula or on the parent bodies. Physical sorting of different dust grains (Regelous et al., 2008) or destruction of thermally labile presolar grains in the nebula (Trinquier et al., 2009) may have selectively excluded certain components from the accretion process. Likewise, aqueous alteration on chondrite parent bodies may have caused a selective modification and redistribution of presolar components (Yokoyama et al., 2011).

Fig. 5 reveals a general decrease of the Mo isotope anomalies over time, as expected for the dynamical evolution of the solar nebula. The largest anomalies were measured for some of the oldest objects, CAI A-ZH-5, while no anomalies were resolved for the terrestrial planets, which were fully accreted much later than the meteorite parent bodies (e.g., Kleine et al., 2009). Among the investigated CAI only A-ZH-5 exhibits an s-process deficiency similar to but much larger than those observed for the meteorite parent bodies. A-ZH-5 thus provides an example of the initial heterogeneity of the solar nebula. In contrast, the excess of r-process isotopes in the other CAI more likely is due to a late injection of neutron-rich material (see above, Section 4.3).

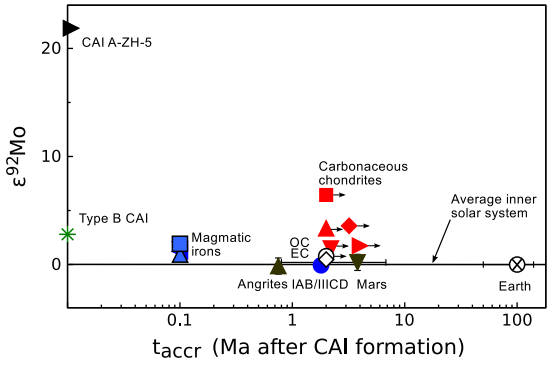

Fig. 5. Mo isotopic anomalies vs. accretion age. Symbols are as in Fig. 1. Data for CAI A-ZH-5, ordinary chondrites (OC), differentiated meteorites, Mars and the Earth reveal an increasing homogenization of the solar nebula over time, as expected from dynamic models of the solar nebula. Carbonaceous chondrites deviate from this trend and exhibit larger Mo isotopic anomalies than expected for their accretion age, probably indicating that they received a greater portion of material from the outer solar system, where mixing and homogenization were slower than closer to the Sun, where the other meteorite parent bodies formed. Note that CAI A-ZH-5 is characterized by a large deficit in s-process isotopes and as such may sample the initial s-process heterogeneity of the inner solar system. Note further that type B CAI are characterized by an excess in r-process isotopes and cannot represent the initial heterogeneity of the solar nebula. Their Mo isotope anomalies more likely reflect a late addition of neutron-rich material (see text for further details). Accretion ages are from Kleine et al. (2009, 2011) and Nyquist et al. (2009). Note that accretion ages for CAI, magmatic irons, non-magmatic irons and angrites overlap within their uncertainties. To avoid overcrowding, these uncertainties are not shown. Arrows indicate that the plotted ages are maximum ages and that accretion could have occurred any time later.

The Mo isotope anomalies of the meteorite parent bodies are intermediate between values for A-ZH-5 and the Earth, as expected for homogenization of the solar nebula over time. However, the Mo isotope anomalies of the bulk meteorites do not only scale with the age of their parent bodies (Fig. 5). Hafnium–tungsten data for magmatic iron meteorites indicate that their parent bodies accreted within less than ~1 Ma after CAI formation (Burkhardt et al., 2008; Kleine et al., 2005; Qin et al., 2008; Scherstén et al., 2006), while the majority of chondrules formed 2–3 Ma after CAI formation, as indicated by Pb–Pb and Al–Mg chronometry (e.g., Krot et al., 2009; Nyquist et al., 2009). Since the chondrite parent bodies must have accreted after formation of the youngest chondrule of a given chondrite group, these ages indicate that the parent bodies of the magmatic irons accreted at least 1–3 Ma earlier than those of the chondrites. Nevertheless, some carbonaceous chondrites have larger Mo isotope anomalies than the magmatic irons, in spite of their late formation.

Carbonaceous chondrites also tend to have larger Mo isotope anomalies than ordinary and enstatite chondrites and this raises the question as to whether these larger anomalies are caused by a higher abundance of refractory inclusions, as is the case for Ti isotopic anomalies observed in carbonaceous chondrites (Trinquier et al., 2009). However, most CAI exhibit Mo isotope anomalies that are smaller than those of the Allende bulk rock, and the Mo isotope pattern of these CAI is distinct from that of Allende and other carbonaceous chondrites. Only CAI A-ZH-5 has a Mo isotope pattern similar to those of the chondrites and the large anomalies of A-ZH-5 suggest that such CAI may be an important component in determining the isotope composition of bulk chondrites. However, assuming that CV chondrites contain ~5% CAI by mass (Hezel et al., 2008), mass balance reveals that nearly two thirds of the CAI in CV chondrites would need to have a composition like A-ZH-5 to account for the observed Mo isotope composition of CV chondrites. This is highly unlikely because CAI such as A-ZH-5 are rare and only one out of the six investigated CAI shows such large Mo isotope anomalies. Note however that CAI with group III REE patterns (such as A-ZH-5) are more common in CM chondrites. If the Mo isotopic composition of these CAI is similar to that of A-ZH-5, then the Mo isotopic composition of CM chondrites may at least in part reflect the presence of such CAI.

Nevertheless, the Mo isotope anomalies of the carbonaceous chondrites provide evidence for a higher-than-expected degree of heterogeneity in the solar nebula at a relatively late time. Carbonaceous chondrites derive from bodies that accreted at greater heliocentric distance than other meteorite parent bodies. Due to longer orbital periods and a decrease in surface density of the solar nebula, the mixing and homogenization timescales within the nebula increase with increasing heliocentric distance. The relatively large isotope anomalies of the carbonaceous chondrites may thus simply reflect a persistent heterogeneity of the disk in the outer part of the inner solar system. Alternatively, carbonaceous chondrites received a greater portion of primitive material from the outer solar system than any other meteorite parent body. It is conceivable that this material was isotopically distinct from material in the inner solar system, such that a late inward transport of outer solar system material could account for the observed isotopic anomalies in the carbonaceous chondrites. Such a model would be consistent with the volatile-rich nature of carbonaceous chondrites and could also account for their pronounced ^{54}Cr anomalies compared to other inner solar system objects (Trinquier et al., 2007). In this context, the correlation of ^{54}Cr and O isotope anomalies in the carbonaceous chondrites can be understood as reflecting the addition of water-bearing material from the outer solar system. Yet another explanation for the Mo isotopic anomalies in the carbonaceous chondrites is that they at least in part reflect selective removal of presolar components as a result of parent body processing. Such effects have been observed for Os isotopes by Yokoyama et al. (2011) and should be a target for future research.

Apart from heliocentric distance and accretion timescale, the parent body size may be important in defining the magnitude of isotope anomalies. Larger bodies integrate material from a broader feeding zone, so that their isotope compositions should be closer to that of the average solar system. The most obvious manifestation of this size-dependence is the isotopic difference between CAI A-ZH-5, which samples a small-scale heterogeneity of the solar nebula, and Earth and Mars, which accreted material over a broad area of the disk. As such, the relatively large Mo isotope anomalies of the carbonaceous chondrites could in principle also reflect the small sizes of their parent bodies compared to those of the differentiated meteorites. Unfortunately, the sizes of the different meteorite parent bodies are not known well enough to test this hypothesis. Nevertheless, for some of the magmatic irons there appears to be an inverse correlation between parent body size and Mo isotope anomalies. Based on metallographic cooling rates the parent body sizes were estimated to increase in the order IVB<IIIAB<IVA (Goldstein et al., 2009; Yang et al., 2010), consistent with a decrease in the Mo isotope anomalies of these iron meteorites.

4.6. Genetic relationships among planetary bodies

Variations in O isotope compositions of meteorites have been used to infer genetic relationships between different meteorite groups (e.g., Clayton and Mayeda, 1996). For instance, O isotope similarities between LL chondrites and IVA irons may indicate that both meteorite groups accreted from similar precursor materials. Likewise, the terrestrial-like O isotope composition of enstatite chondrites was used to argue for formation of the Earth from this group of chondrites (Javoy et al., 2010). The nucleosynthetic Mo isotope anomalies in bulk meteorites provide an important test for such proposed genetic relationships because samples from a common parent body must have identical Mo isotope compositions.

Table 2 summarizes proposed genetic relationships among planetary objects. Some of these relationships (e.g., IAB–IIICD irons; IIE irons–H chondrites) are consistent with the Mo isotope data. However, a common parent body for IVB irons and angrites, CR chondrites and Tafassasset, and CV chondrites and the Eagle Station pallasite can be excluded based on the Mo isotope data.

4.7. Origin of Earth's building blocks

Since all groups of chondrites investigated here, and also most other meteorites are characterized by a deficit in s-process Mo isotopes, they

Table 2
Genetic links between meteorite groups.

Proposed genetic link	Reference	Relation supported by Mo isotopic data
IAB–IIICD irons	Choi et al., 1995	Yes
IIE irons–H chondrites	Clayton and Mayeda, 1996; McDermott et al., 2011	Yes
IIIAB irons–main group pallasites	Clayton and Mayeda, 1996; Wasson and Choi, 2003	Yes
IVA irons–L-LL chondrites	Clayton and Mayeda, 1996; Wang et al., 2004	Yes
IVB irons–angrites	Campbell and Humayun, 2005	No
CV/CO chondrites–[a] Eagle Station pallasites	Clayton and Mayeda, 1996; Shukolyukov and Lugmair, 2006	No
CR chondrites–Tafassasset	Bourot-Denise et al., 2002	No

[a] Mo isotope anomalies of the Eagle Station pallasite are distinct from other bulk meteorites in that they cannot be satisfactorily fitted by a s-process deficit alone. An additional excess in r-process isotopes is required, which may indicate that the Eagle Station parent body accreted from material enriched in CAI, which often are characterized by r-process enrichments. This hypothesis is consistent with the strongly negative Δ^{17}O of the Eagle Station pallasite (Clayton and Mayeda, 1996).

cannot represent the average building blocks of the Earth. The only meteorites with terrestrial-like Mo isotope compositions are the IAB–IIICD irons and angrites, but these have non-terrestrial O isotope compositions and so cannot be representative of Earth's building blocks.

The Mo isotope data, thus, show that the Earth on average accreted from material different from known types of meteorites. This observation is not surprising because the Earth assembled from objects that dominantly originated in the inner solar system, whereas the meteorite parent bodies accreted from material that probably always had been in an orbit beyond Mars. Evidently, the meteorites received a greater portion of material from greater heliocentric distance as the average material forming the Earth, which is characterized by an enrichment in s-process isotopes of Mo compared to the material forming the meteorite parent bodies. Such a heliocentric gradient is consistent with the relatively large Mo isotope anomalies in the carbonaceous chondrites, which formed at greater heliocentric distance than any other meteorites and have the largest deficits in s-process isotopes among the meteorites.

The observation that chondrites cannot be the main building blocks of the Earth has important implications for interpreting the ^{142}Nd deficit of chondrites relative to the accessible Earth (Boyet and Carlson, 2005). Fig. 6 reveals that ^{142}Nd and ^{92}Mo anomalies in ordinary, enstatite and CI chondrites plot along a trend that is consistent with deficits in s-process isotopes in these chondrites. However, CV and CM chondrites do not plot on this correlation line but seem to define a second trend passing through the data point for CI chondrites. This second trend cannot readily be accounted for by variations in p-, s- and r-process isotopes, indicating that the Nd and Mo isotopic anomalies seem to be decoupled in the carbonaceous chondrites. Nevertheless, the trend defined by the ordinary, enstatite and CI chondrites passes through the terrestrial Nd and Mo isotope compositions, which would suggest the ^{142}Nd difference between the accessible Earth and chondrites to be nucleosynthetic. However, a correlation of ^{142}Nd and ^{148}Nd in chondrites reveals a ~20 ppm ^{142}Nd deficit in chondrites at a terrestrial ^{148}Nd abundance, arguing against a nucleosynthetic origin of the ^{142}Nd difference between chondrites and the accessible Earth (Carlson et al., 2007). The significance of the ^{92}Mo–^{142}Nd covariation thus remains unclear but should be a target of future research.

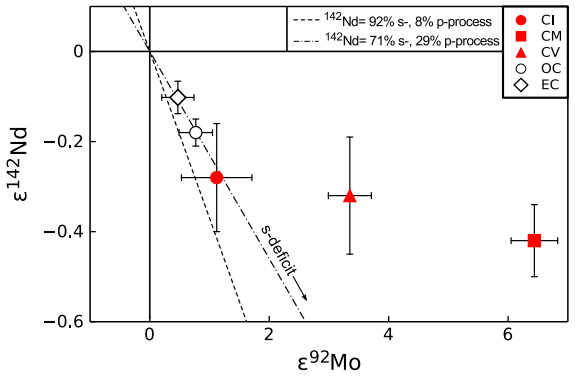

Fig. 6. Plot of ε^{92}Mo vs. ε^{142}Nd for chondrites. Nd isotopic data for chondrites are from Carlson et al. (2007) and Gannoun et al. (2011). Plotted are means for each chondrite group. Errors were calculated using $\sigma t_{0.95,n-1}/\sqrt{n}$ (see Table 1). The dashed line is a mixing line between the terrestrial composition and an average s-process component (Arlandini et al., 1999). Note however that the stellar model of Arlandini et al. (1999) is known to overproduce ^{142}Nd; the dash-dotted line is a mixing line calculated assuming a lower s-process contribution to ^{142}Nd (see also Gannoun et al., 2011). Mo and Nd isotopic anomalies correlate for enstatite, ordinary and CI chondrites and plot along the calculated mixing lines. CV and CM chondrites deviate from this trend, indicating a decoupling of the Nd and Mo isotopic anomalies in these samples. The combined Nd and Mo isotopic data suggest that the ^{142}Nd deficits of chondrites relative to the accessible Earth should not only be evaluated as a signature of early planetary differentiation but also by considering a nucleosynthetic origin.

5. Conclusions

The Mo isotopic data reveal planetary-scale nucleosynthetic isotopic heterogeneities in the solar system that are caused by incomplete homogenization of s-process carriers within the solar nebula, consistent with findings by Dauphas et al. (2002b, 2004). The Mo isotope anomalies generally decrease over time, reflecting an increasing homogenization of the solar nebula. However, carbonaceous chondrites exhibit Mo isotopic anomalies that are larger than expected for their relatively late accretion, most likely caused by a late addition of primitive material from the outer solar system. This is consistent with the volatile-rich nature of carbonaceous chondrites and can account for their characteristic ^{54}Cr–Δ^{17}O correlation. Collectively the Mo isotopic data are consistent with dynamical models of the solar nebula, as these predict an increasing homogenization of the nebula over time and a late inward transport of material from the outer solar system.

All meteorites are depleted in s-process Mo isotopes relative to the Earth, indicating that Earth on average accreted from material that is different from known types of meteorites. Material in the inner solar system thus consists of a different mixture of stellar-derived dust than material dominating beyond the orbit of Mars. Consequently, chondrites may not be a suitable reference for the isotopic composition of the Earth. The observation that ^{92}Mo and ^{142}Nd anomalies are roughly correlated in chondrites shows that the ^{142}Nd deficit of chondrites relative to the accessible Earth may not unequivocally be due to an early differentiation of the Earth. However, further work is needed to elucidate the isotopic composition of the Earth in comparison to chondrites in more detail.

Acknowledgments

This work was supported by the SNF (no. 2-77213-08). We thank Fred Ciesla for providing insights into the dynamical evolution of the solar nebula, Richard Walker and Nicolas Dauphas for discussions and constructive reviews and Richard Carlson for his helpful comments and editorial efforts.

Appendix A. Supplementary data

Supplementary data to this article can be found online at doi:10.1016/j.epsl.2011.10.010.

References

Amari, S., Hoppe, P., Zinner, E., Lewis, R.S., 1995. Trace-element concentrations in single circumstellar silicon carbide grains from the Murchison meteorite. Meteoritics 30, 679–693.
Andreasen, R., Sharma, M., 2006. Solar nebula heterogeneity in p-process samarium and neodymium isotopes. Science 314, 806–809.
Andreasen, R., Sharma, M., 2007. Mixing and homogenization in the early solar system: clues from Sr, Ba, Nd, and Sm isotopes in meteorites. Astrophys. J. 665, 874–883.
Arlandini, C., Kappeler, F., Wisshak, K., Gallino, R., Lugaro, M., Busso, M., Straniero, O., 1999. Neutron capture in low-mass asymptotic giant branch stars: cross sections and abundance signatures. Astrophys. J. 525, 886–900.
Becker, H., Walker, R.J., 2003a. In search of extant Tc in the early solar system: Ru-98 and Ru-99 abundances in iron meteorites and chondrites. Chem. Geol. 196, 43–56.
Becker, H., Walker, R.J., 2003b. Efficient mixing of the solar nebula from uniform Mo isotopic composition of meteorites. Nature 425, 152–155.
Birck, J.L., Allègre, C.J., 1984. Chromium isotopic anomalies in Allende refractory inclusions. Geophys. Res. Lett. 11, 943–946.
Birck, J., Lugmair, G., 1988. Nickel and chromium isotopes in Allende inclusions. Earth Planet. Sci. Lett. 90, 131–143.
Boss, A.P., 2008. Mixing in the solar nebula: implications for isotopic heterogeneity and large-scale transport of refractory grains. Earth Planet. Sci. Lett. 268, 102–109.
Bourot-Denise, M., Zanda, B., Javoy, M., 2002. Tafassasset: an equilibrated CR chondrite. Lunar Planet. Sci. Conf. 33, 1611.
Boyet, M., Carlson, R.W., 2005. ^{142}Nd evidence for early (>4.53 Ga) global differentiation of the silicate Earth. Science 309, 576–581.
Burbidge, E.M., Burbidge, G.R., Fowler, W.A., Hoyle, F., 1957. Synthesis of the elements in stars. Rev. Mod. Phys. 29, 547–650.
Burkhardt, C., Kleine, T., Bourdon, B., Palme, H., Zipfel, J., Friedrich, J.M., Ebel, D.S., 2008. Hf–W mineral isochron for Ca, Al-rich inclusions: age of the solar system and the

timing of core formation in planetesimals. Geochim. Cosmochim. Acta 72, 6177–6197.
Burkhardt, C., Kleine, T., Dauphas, N., Oberli, F., Wieler, R., 2011. Nucleosynthetic Mo isotope anomalies in acid leachates of the Murchison chondrite and their relevance for early solar system processes. Lunar Planet. Sci. Conf. 42 #2592.
Campbell, A.J., Humayun, M., 2005. Compositions of group IVB iron meteorites and their parent melt. Geochim. Cosmochim. Acta 69, 4733–4744.
Carlson, R.W., Boyet, M., Horan, M., 2007. Chondrite barium, neodymium, and samarium isotopic heterogeneity and early Earth differentiation. Science 316, 1175–1178.
Chen, J.H., Papanastassiou, D.A., Wasserburg, G.J., 2010. Ruthenium endemic isotope effects in chondrites and differentiated meteorites. Geochim. Cosmochim. Acta 74, 3851–3862.
Choi, B., Ouyang, X., Wasson, J., 1995. Classification and origin of IAB and IIICD iron-meteorites. Geochim. Cosmochim. Acta 59, 593–612.
Ciesla, F.J., 2009. Two-dimensional transport of solids in viscous protoplanetary disks. Icarus 200, 655–671.
Clayton, R.N., Mayeda, T.K., 1996. Oxygen isotope studies of achondrites. Geochim. Cosmochim. Acta 60, 1999–2017.
Dauphas, N., Marty, B., Reisberg, L., 2002a. Molybdenum nucleosynthetic dichotomy revealed in primitive meteorites. Astrophys. J. 569, 139–142.
Dauphas, N., Marty, B., Reisberg, L., 2002b. Molybdenum evidence for inherited planetary scale isotope heterogeneity of the protosolar nebula. Astrophys. J. 565, 640–644.
Dauphas, N., Marty, B., Reisberg, L., 2002c. Inference on terrestrial genesis from molybdenum isotope systematics. Geophys. Res. Lett. 29(6), 1084. doi:10.1029/2001GL014237.
Dauphas, N., Davis, A.M., Marty, B., Reisberg, L., 2004. The cosmic molybdenum–ruthenium isotope correlation. Earth Planet. Sci. Lett. 226, 465–475.
Dauphas, N., Cook, D.L., Sacarabany, A., Fröhlich, C., Davis, A.M., Wadhwa, M., Pourmand, A., Rauscher, T., Gallino, R., 2008. Iron 60 evidence for early injection and efficient mixing of stellar debris in the protosolar nebula. Astrophys. J. 686, 560–569.
Fujii, T., Moynier, F., Telouk, P., Albarede, F., 2006. Mass-independent isotope fractionation of molybdenum and ruthenium and the origin of isotopic anomalies in Murchison. Astrophys. J. 647, 1506–1516.
Gannoun, A., Boyet, M., Rizo, H., El Goresy, A., 2011. ^{146}Sm–^{142}Nd systematics measured in enstatite chondrites reveals a heterogeneous distribution of ^{142}Nd in the solar nebula. PNAS 108, 7693–7697.
Goldstein, J.I., Scott, E.R.D., Chabot, N.L., 2009. Iron meteorites: crystallization, thermal history, parent bodies, and origin. Chem. Erde/Geochemistry 69, 293–325.
Hezel, D.C., Russell, S.S., Ross, A.J., Kearsley, A.T., 2008. Modal abundances of CAIs: implications for bulk chondrite element abundances and fractionations. Meteorit. Planet. Sci. 43, 1879–1894.
Javoy, M., Kaminski, E., Guyot, F., Andrault, D., Sanloup, C., Moreira, M., Labrosse, S., Jambon, A., Agrinier, P., Davaille, A., Jaupart, C., 2010. The chemical composition of the Earth: enstatite chondrite models. Earth Planet. Sci. Lett. 293, 259–268.
Kashiv, Y., Cai, Z., Lai, B., Sutton, S.R., Lewis, R.S., Davis, A.M., Clayton, R.N., Pellin, M.J., 2001. Synchrotron X-ray fluorescence: a new approach for determining trace element concentrations in individual presolar SiC grains. Lunar Planet. Sci. Conf. 32, 2192.
Kleine, T., Mezger, K., Palme, H., Scherer, E., Münker, C., 2005. Early core formation in asteroids and late accretion of chondrite parent bodies: evidence from ^{182}Hf–^{182}W in CAIs, metal-rich chondrites, and iron meteorites. Geochim. Cosmochim. Acta 69, 5805–5818.
Kleine, T., Touboul, M., Bourdon, B., Nimmo, F., Mezger, K., Palme, H., Jacobsen, S.B., Yin, Q., Halliday, A.N., 2009. Hf–W chronology of the accretion and early evolution of asteroids and terrestrial planets. Geochim. Cosmochim. Acta 73, 5150–5188.
Kleine, T., Hans, U., Irving, A.J., Bourdon, B., 2011. Hf–W chronometry of angrites: implication for ^{26}Al heterogeneity and core formation in protoplanets. Goldschmidt Conference 2011, p. 1199.
Krot, A.N., Amelin, Y., Bland, P., Ciesla, F.J., Connelly, J., Davis, A.M., Huss, G.R., Hutcheon, I.D., Makide, K., Nagashima, K., Nyquist, L.E., Russell, S.S., Scott, E.R.D., Thrane, K., Yurimoto, H., Yin, Q., 2009. Origin and chronology of chondritic components: a review. Geochim. Cosmochim. Acta 73, 4963–4997.
Lu, Q., Masuda, A., 1994. The isotopic composition and atomic weight of molybdenum. Int. J. Mass Spectrom. Ion Processes 130, 65–72.
McCulloch, M.T., Wasserburg, G.J., 1978. Barium and neodymium isotopic anomalies in the Allende meteorite. Astrophys. J. 220, 15–19.
McDermott, K.H., Greenwood, R.C., Franchi, I.A., Anand, M., Scott, E.R.D., 2011. Oxygen isotopic and petrological constraints on the origin and relationship of IIE iron meteorites and H chondrites. Lunar Planet. Sci. Conf. 42, 2563.
Nicolussi, G.K., Pellin, M.J., Lewis, R.S., Davis, A.M., Amari, S., Clayton, R.N., 1998. Molybdenum isotopic composition of individual presolar silicon carbide grains from the Murchison meteorite. Geochim. Cosmochim. Acta 62, 1093–1104.
Niemeyer, S., Lugmair, G.W., 1981. Ubiquitous isotopic anomalies in Ti from normal Allende inclusions. Earth Planet. Sci. Lett. 53, 211–225.
Nittler, L.R., 2003. Presolar stardust in meteorites: recent advances and scientific frontiers. Earth Planet. Sci. Lett. 209, 259–273.
Nyquist, L.E., Kleine, T., Shih, C.Y., Reese, Y.D., 2009. The distribution of short-lived radioisotopes in the early solar system and the chronology of asteroid accretion, differentiation, and secondary mineralization. Geochim. Cosmochim. Acta 73, 5115–5136.
Pack, A., Kremer, K., Albrecht, N., Simon, K., Kronz, A., 2010. Description of an aerodynamic levitation apparatus with applications in earth sciences. Geochem. Trans. 11, 4.
Qin, L., Dauphas, N., Wadhwa, M., Markowski, A., Gallino, R., Janney, P.E., Bouman, C., 2008. Tungsten nuclear anomalies in planetesimal cores. Astrophys. J. 674, 1234–1241.
Qin, L., Alexander, C.M.O'.D., Carlson, R.W., Horan, M.F., Yokoyama, T., 2010. Contributors to chromium isotope variations of meteorites. Geochim. Cosmochim. Acta 74, 1122–1145.
Regelous, M., Elliott, T., Coath, C.D., 2008. Nickel isotope heterogeneity in the early solar system. Earth Planet. Sci. Lett. 272, 330–338.
Scherstén, A., Elliott, T., Hawkesworth, C., Russell, S., Masarik, J., 2006. Hf W evidence for rapid differentiation of iron meteorite parent bodies. Earth Planet. Sci. Lett. 241, 530–542.
Schönbächler, M., Lee, D.C., Rehkämper, M., Halliday, A.N., Fehr, M.A., Hattendorf, B., Günther, D., 2003. Zirconium isotope evidence for incomplete admixing of r-process components in the solar nebula. Earth Planet. Sci. Lett. 216, 467–481.
Shukolyukov, A., Lugmair, G.W., 2006. Manganese chromium isotope systematics of carbonaceous chondrites. Earth Planet. Sci. Lett. 250, 200–213.
Sprung, P., Scherer, E.E., Upadhyay, D., Leya, I., Mezger, K., 2010. Non-nucleosynthetic heterogeneity in non-radiogenic stable Hf isotopes: implications for early solar system chronology. Earth Planet. Sci. Lett. 295, 1–11.
Trinquier, A., Birck, J.L., Allègre, C.J., 2007. Widespread ^{54}Cr heterogeneity in the inner solar system. Astrophys. J. 655, 1179–1185.
Trinquier, A., Elliott, T., Ulfbeck, D., Coath, C., Krot, A.N., Bizzarro, M., 2009. Origin of nucleosynthetic isotope heterogeneity in the solar protoplanetary disk. Science 324, 374–376.
Wallerstein, G., Iben Jr., I., Parker, P., Boesgaard, A.M., Hale, G.M., Champagne, A.E., Barnes, C.A., Käppeler, F., Smith, V.V., Hoffman, R.D., Timmes, F.X., Sneden, C., Boyd, R.N., Meyer, B.S., Lambert, D.L., 1997. Synthesis of the elements in stars: forty years of progress. Rev. Mod. Phys. 69, 995–1084.
Wang, P.L., Rumble, D., McCoy, T.J., 2004. Oxygen isotopic compositions of IVA iron meteorites: implications for the thermal evolution derived from in situ ultraviolet laser microprobe analyses. Geochim. Cosmochim. Acta 68, 1159–1171.
Wasson, J.T., Choi, B.G., 2003. Main-group pallasites — chemical composition, relationship to IIIAB irons, and origin. Geochim. Cosmochim. Acta 67, 3079–3096.
Yang, J., Goldstein, J.I., Michael, J.R., Kotula, P.G., Scott, E.R.D., 2010. Thermal history and origin of the IVB iron meteorites and their parent body. Geochim. Cosmochim. Acta 74, 4493–4506.
Yin, Q., Jacobsen, S.B., Yamashita, K., 2002. Diverse supernova sources of pre-solar material inferred from molybdenum isotopes in meteorites. Nature 415, 881–883.
Yokoyama, T., Rai, V.K., Alexander, C.M.O., Lewis, R.S., Carlson, R.W., Shirey, S.B., Thiemens, M.H., Walker, R.J., 2007. Osmium isotope evidence for uniform distribution of s- and r-process components in the early solar system. Earth Planet. Sci. Lett. 259, 567–580.
Yokoyama, T., Alexander, C.M.O., Walker, R.J., 2010. Osmium isotope anomalies in chondrites: results for acid residues and related leachates. Earth Planet. Sci. Lett. 291, 48–59.
Yokoyama, T., Alexander, C.M.O., Walker, R.J., 2011. Assessment of nebular versus parent body processes on presolar components present in chondrites: evidence from osmium isotopes. Earth Planet. Sci. Lett. 305, 115–123.